

Comparison of two constructions of hybrid magnetic bearings

Abstract. The paper presents a comparative analysis of two various constructions of the hybrid magnetic bearings. For this purpose, the basic parameters of the magnetic bearings were defined. Additionally, new parameters are proposed in order to estimate nonlinearity of the magnetic force and cross-coupling between axes. Comparison of the magnetic bearing constructions was performed using 3 dimensional simulation models.

Streszczenie. W artykule przedstawiono analizę porównawczą dwóch różnych konstrukcji hybrydowych łożysk magnetycznych. W tym celu, zdefiniowano podstawowe parametry wykorzystywane do opisu łożysk magnetycznych. Dodatkowo, zaproponowano nowe parametry w celu oszacowania nieliniowości siły magnetycznej oraz sprzężenia między osiami. Porównanie konstrukcji łożysk magnetycznych wykonano w oparciu o analizę 3 wymiarowych modeli symulacyjnych. (Porównanie dwóch konstrukcji hybrydowych łożysk magnetycznych).

Keywords: permanent magnets excited magnetic bearing, finite element analysis, parameters of the magnetic bearing.

Słowa kluczowe: łożysko magnetyczne wzbudzone magnesami trwałymi, analiza metodą elementów skończonych, parametry łożyska magnetycznego.

Introduction

Magnetic bearings (MBs) use the magnetic field to levitate the rotor without mechanical contact. Therefore, MBs are more often installed in high speed rotating machines due to their unique properties like the absence of lubrication and contaminating wear, low losses, online diagnostics, a vibration damper [1, 2]. There are various classifications of the magnetic bearings [3]. One categorization classifies them into radial magnetic bearings [4, 5] and axial magnetic bearings [6, 7]. Different classification divides MBs into active magnetic bearings, passive magnetic bearings and active magnetic bearings with permanent magnets also called hybrid magnetic bearings (HMBs) [4, 8-13].

The magnetic force generated by the MB is nonlinear, therefore the bias flux is used to linearize the magnetic force characteristic with respect to the control current and position of the rotor [3]. In active magnetic bearings, the bias flux is generated by the bias current that flows through all windings. Unfortunately, the flow of the bias current causes significant power losses. An alternative method of the bias flux generation is the usage of permanent magnets employed in HMBs [11, 14-17]. According to the authors [18], a 6-pole HMB uses 86.65% less electricity than an 8-pole active magnetic bearing with the same load capacity. The 6-pole construction of the MB in comparison to an 8-pole can be supplied by three-phase inverters, which reduces manufacturing costs [18]. Unfortunately, the 6-pole HMB has the significantly nonlinear characteristic of the magnetic force in the y -axis as well as the cross-coupling effect between axes [18-20].

The aim of this paper is to present a comparative analysis of two constructions of the HMBs and to indicate the construction that has lower nonlinearity of the magnetic force and smaller cross-coupling effect. Both variants have the same geometry parameters such as the outer diameter of the stator, the inner diameter of the stator, the air gap and length of the stator. All parameters of the MBs were obtained from 3D simulation models prepared in Ansoft Maxwell 3D software [21].

Description of the HMB constructions

Fig. 1.a and 1.b present geometry of two variants of the HMB constructions. Both variants of the HMB have six salient poles. Version A of the HMB has three wound poles and three poles with permanent magnets installed in cut holes of the poles. The version B of the HMB has six wound poles, while six permanent magnets are installed in cut holes of the back-iron. Both variants of the HMB have

installed permanent magnets NdFeB (N38, $B_r = 1.23$ T, $H_c = 963800$ A/m), magnetized along the shortest edge, to provide the bias magnetic flux that determines the operating point of the magnetic circuit. The installation of permanent magnets in cut spaces of cores ensures the precise fabrication of the stators.

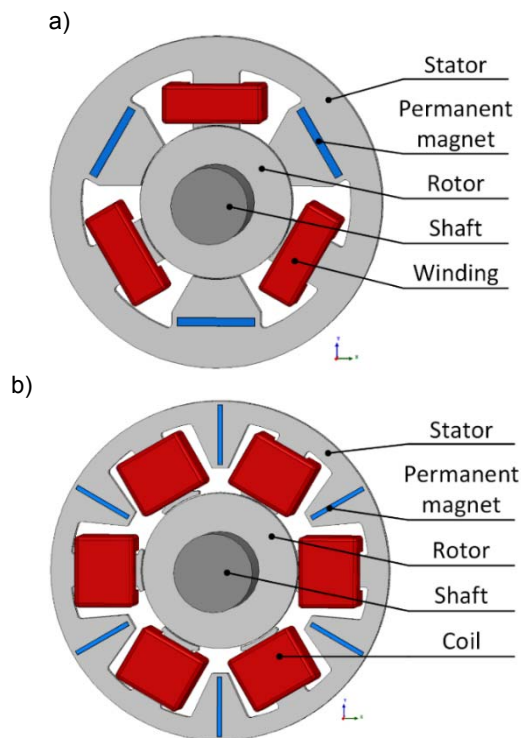


Fig.1. Geometry of the magnetic bearing with permanent magnets: a) variant A, b) variant B.

The stator and the rotor are made of the dynamo steel sheet M400-50A, which is 0.5 mm width. Usage of the laminated cores significantly reduces eddy currents as well as lowers power losses in the magnetic circuit. Turns number of each winding for version A of the HMB is equal to 100, whereas turns number of each coil for version B of the HMB is equal to 100. For the variant B of the HMB, two coils are connected in series to create one winding. The cross-sectional area of the winding slot for the version A of the HMB equals ca. 194 mm^2 , while for the version B of the HMB amounts to ca. 129 mm^2 . Assuming that the slot fill factor is equal to 0.4, the resistance of variant A amounts to $266 \text{ m}\Omega$, while the resistance of the of variant B equals

400 mΩ. The length of the air gap equals 0.3 mm and it is identical for both variants of the HMB. The main dimensions of both versions of the HMB are presented in Fig. 2.a and 2.b. The length of the stator for both variants equals 10 mm.

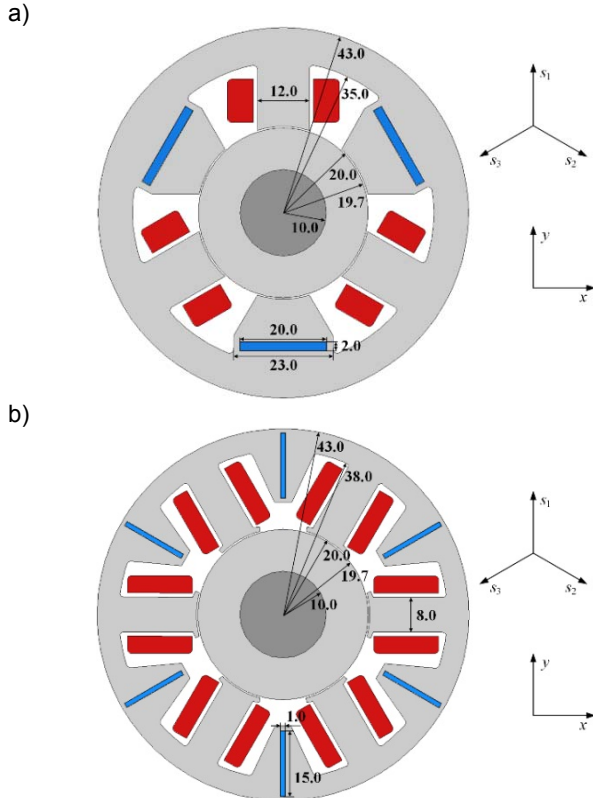


Fig. 2. Main dimensions of the HMB: a) variant A, b) variant B

These two variants of the HMBs can be controlled in three axes (s_1, s_2, s_3) as well as in two axes (x and y) [22]. Widely used in the rotating machine industry, a control system of the magnetic bearing measures position of the rotor in two axes. Therefore, parameters for both versions of HMBs are calculated for the x and y -axis. Winding currents i_1, i_2, i_3 can be calculated from control currents i_x, i_y according to the following expressions:

$$(1.a) \quad i_1 = i_y$$

$$(1.b) \quad i_2 = -\frac{1}{2}i_y + \frac{\sqrt{2}}{3}i_x$$

$$(1.c) \quad i_3 = -\frac{1}{2}i_y - \frac{\sqrt{2}}{3}i_x$$

Parameters of the magnetic bearing

Magnetic bearings belong to special machines that are described by specific parameters. These parameters include position stiffness k_s , current stiffness k_i , dynamic inductance L_d and velocity induced voltage e_v [23]. Some magnetic bearings do not have the same value of stiffness in the x - and y -axis, therefore these parameters are given separately for both axes. The position stiffness k_{sx} and k_{sy} are calculated as the derivative of the magnetic force with respect to the rotor position:

$$(2.a) \quad k_{sx} = \left. \frac{\partial F_x}{\partial x} \right|_{x=0, i_x=0}$$

$$(2.b) \quad k_{sy} = \left. \frac{\partial F_y}{\partial y} \right|_{y=0, i_y=0}$$

The current stiffness k_{ix} and k_{iy} are calculated as the derivative of the magnetic force with respect to the control current:

$$(3.a) \quad k_{ix} = \left. \frac{\partial F_x}{\partial i_x} \right|_{x=0, i_x=0}$$

$$(3.b) \quad k_{iy} = \left. \frac{\partial F_y}{\partial i_y} \right|_{y=0, i_y=0}$$

The dynamic inductance L_d is calculated as the derivative of linkage flux Ψ_k with respect to the winding current i_k :

$$(4) \quad L_{dk} = \frac{\partial \Psi_k}{\partial i_k}$$

where k denotes the winding number $k \in \{1, 2, 3\}$. The velocity induced voltage e_v is calculated as the derivative of linkage flux Ψ_k with respect to the rotor position s_k :

$$(5) \quad e_{vk} = \frac{\partial \Psi_k}{\partial s_k}$$

Often, magnetic forces generated by the magnetic bearing are described by the following linear equations:

$$(6.a) \quad F_x(x, i_x) = k_{sx}x + k_{ix}i_x$$

$$(6.b) \quad F_y(y, i_y) = k_{sy}y + k_{iy}i_y$$

Eq. 6.a and 6.b are commonly used to develop a model of the magnetic bearing for purposes of the control system [24]. Unfortunately, these equations assume constant values of the position and current stiffness. As well, these equations neglect the cross-coupling between axes. Therefore, two parameters like the magnetic force nonlinearity factor h_{non} and the cross-coupling factor h_c are proposed for magnetic bearings parameters. The magnetic force nonlinearity factors h_{non} for the x - and y -axis are calculated as mean absolute errors (MAEs) between the magnetic forces and their linear approximation (Eq. 6.a and 6.b):

$$(7.a) \quad h_{xnon} = \frac{1}{n} \sum_x \sum_{i_x} |F_x(x, i_x) - (k_{sx}x + k_{ix}i_x)|$$

$$(7.b) \quad h_{ynon} = \frac{1}{n} \sum_y \sum_{i_y} |F_y(y, i_y) - (k_{sy}y + k_{iy}i_y)|$$

where n denotes the number of calculation points.

The cross-coupling factors h_c for the x - and y -axis are calculated as:

$$(7.a) \quad h_{xc} = \frac{1}{n} \sum_y \sum_{i_y} |F_x(y, i_y)|$$

$$(7.b) \quad h_{yc} = \frac{1}{n} \sum_x \sum_{i_x} |F_y(x, i_x)|$$

Values of current and position stiffness are not constant for the entire operating range, therefore two additional parameters of magnetic bearings were proposed: the initial magnetic force and the maximal magnetic force. The initial magnetic forces F_{x0} and F_{y0} are defined as magnetic forces generated for minimal positions of the rotor and maximal control currents. The maximal magnetic forces F_{xmax} and F_{ymax} are defined as magnetic forces generated for the central position of the rotor and maximal control currents.

Simulation models

Fig. 3 depicts a 3 dimensional finite element model (3D FEM) for variant A of the HMB prepared in Ansoft Maxwell 3D software. A similar simulation model was prepared for the variant B. The 3D FEM had to be used for simulation of the magnetic field, instead of the 2D FEM, because the length of the end windings is longer than the stator length. Therefore, significant leakage flux is omitted in the 2D simulation model that factors in the value of the magnetic force. To decrease the number of tetrahedral elements for the FEM and to limit the calculation time, only half of the HMB geometry was simulated. The simulation model was enclosed by the rectangular shape, which faces are spaced 40 mm from the stator and rotor, except for the symmetry plane that was in the middle of the stator length. The zero Dirichlet boundary condition was set on the outer surface of the simulation model, while the zero Neumann boundary condition is assumed on the symmetry plane.

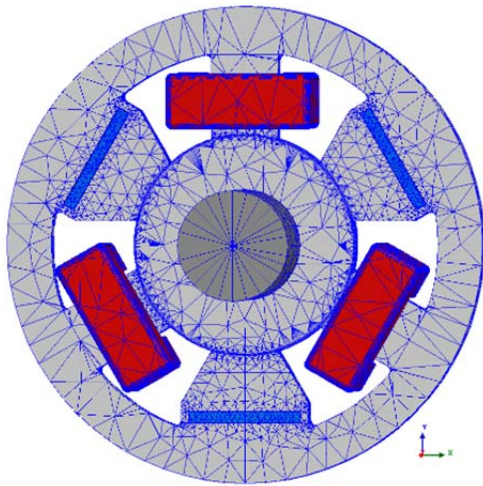


Fig. 3. The finite element model for version A of the HMB.

Calculation domains were discretised using adaptive meshing procedure in order to obtain the fine mesh. The adaptive meshing procedure implemented in Maxwell 3D software has two parameters: the maximal energy error and the maximum number of passes. For every simulation, the maximal energy error was set to 0.5% and the maximum number of passes was set to 15. The adaptive meshing procedure required maximally 7 passes to achieve energy error less than 0.5%. The total number of elements slightly changes with the rotor position, but it fluctuated around 120 000 elements. Tab. 1. presents number of tetrahedral elements in calculation domains for the central position of the rotor and lack of control currents.

Table 1. Number of elements in calculation domains

Calculation domain	Number of elements
Windings	6256
Stator	24572
Rotor	6530
Shaft	545
Permanent magnets	4602
Air gap	13312
Region surrounding the model	49491

Lamination of the stator and rotor cores significantly reduces eddy currents, therefore the simulation model includes magnetostatic calculations with the nonlinear B-H curve of the magnetic material M400-50A. The B-H curve was tested with a closed magnetic circuit [25]. It is difficult to evaluate demagnetization of the permanent magnets, therefore this effect was neglected in simulation models.

The magnetic forces F_x , F_y were calculated from the virtual work method:

$$(8.a) \quad F_x = \left. \frac{\partial W_{co}}{\partial x} \right|,$$

$$(8.b) \quad F_y = \left. \frac{\partial W_{co}}{\partial y} \right|.$$

where W_{co} indicates the coenergy of the HMB.

Magnetic flux linkage ψ was obtained from the following equation:

$$(9) \quad \psi = N \iint_S \vec{B} \cdot d\vec{S},$$

where N is the turn number of the stator windings and S denotes the area of the pole.

The magnetic field simulation, as well as working principles of variant A of the HMB, are presented in the paper [26].

Simulation results

Fig. 4.a and Fig. 4.b present magnetic field distributions for both variants of the HMB for the central position of the rotor and lack of the control current. For this work condition, the premagnetization magnetic field density for the magnetic circuit of stator and rotor can be assessed. It can be noticed that value of the magnetic field density in the stator core for the variant A of the HMB is lower ($B = 0.637$ T inside the wounded pole) than for the variant B ($B = 0.788$ T inside the pole). For both versions of the HMB, value of the premagnetization magnetic field density accounts for about the half of the knee value for the magnetic material M400-50A that is equal to 1.4 T.

Also, both figures indicate that saturation of the magnetic material occurs in the proximity of the permanent magnets. The reason for that is partial short-circuit of the flux generated by permanent magnets. This phenomenon could be reduced by removing sections of the magnetic circuit that are responsible for the short-circuit. Although, division of the stator into few parts significantly hinder the precise assembly of the stator. For that state, the magnetic force generated by the HMBs equals 0 N.

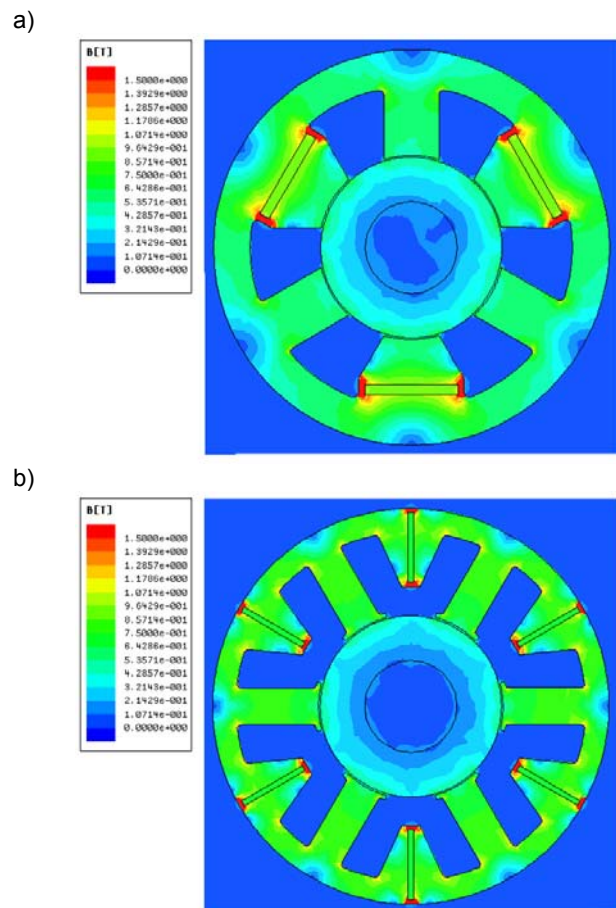


Fig. 4. The magnetic field distribution for the central position of the rotor and lack of control currents: a) variant A, variant B.

In Fig. 5.a and Fig. 5.b are presented magnetic field distributions for both variants of the HMB for the position of the rotor in the y -axis equals -0.2 mm and the control current i_y equals 2 A. This working condition occurs when the control system tries to lift the shaft from its rest position and defines the weight of the rotor that can be lifted. For variant A of the HMB change of the control current i_y causes a change of the magnetic field in wounded poles, while the magnetic field density in poles with permanent magnets is almost constant.

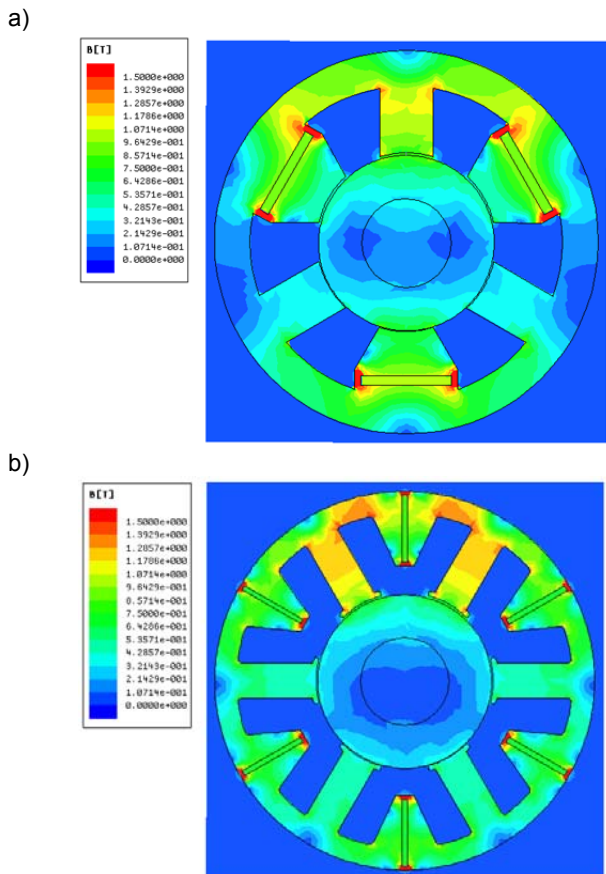


Fig. 5. The magnetic field distribution for the central position of the rotor and the control current i_y equals 2 A: a) variant A, variant B.

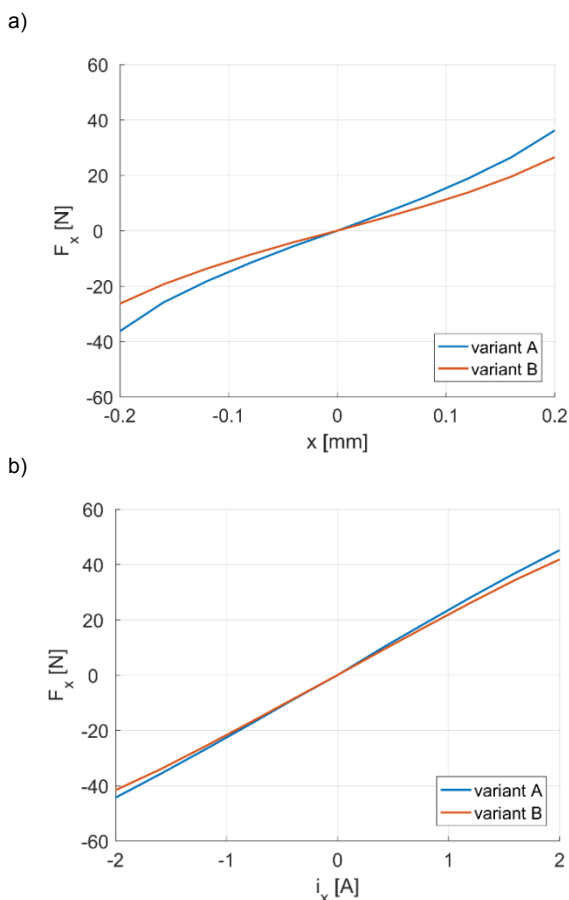


Fig. 6. The magnetic force F_x in the function of the rotor position x (a) and the control current i_x (b) for both versions of the HMB.

The magnetic force F_y generated by variant A for this working condition equals to 13.56 N. Variant B of the HMB has all poles wound and permanent magnets are installed in the back-iron of the stator. Therefore, change of the control current i_y causes a change of the magnetic field in all poles. The magnetic force F_y generated by variant B for this working condition equals to 22.53 N. For both variants of the HMB, the magnetic field density in upper poles is similar and equals for the variant A: 1.405 T and for the variant B: 1.388 T.

Fig. 6.a presents the magnetic force F_x with respect to the rotor position x , while Fig. 6.b depicts the magnetic force F_x in the function of the control current i_x for both variants of the HMB. Both figures indicate that variant B of the HMB has a smaller value of the position and current stiffness in relation to the variant A.

Fig. 7.a presents the magnetic force F_y for both variants of the HMB in the function of the rotor position y (a) and the control current i_y (b). These figures depict significant nonlinearity of the magnetic force for the variant A of the HMB.

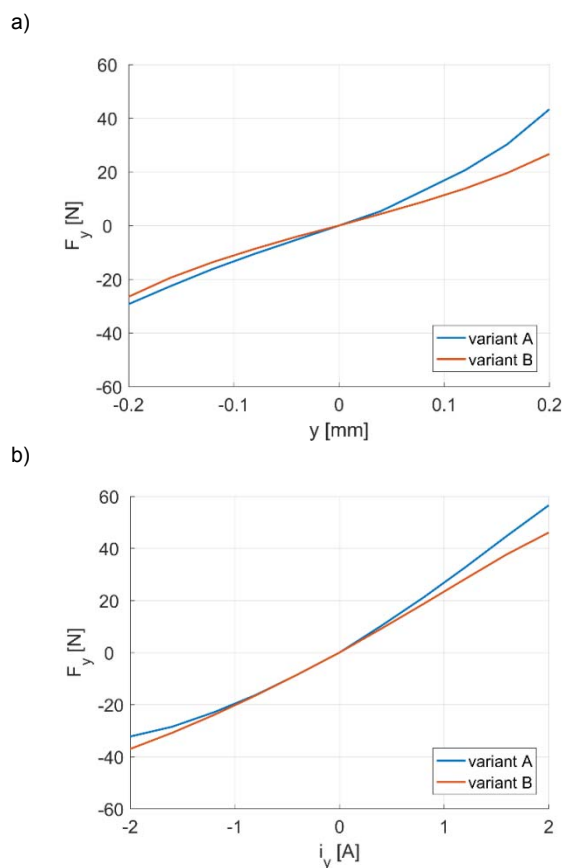


Fig. 7. The magnetic force F_y in function of the rotor position y (a) and the control current i_y (b) for both versions of the HMB.

Fig. 8 indicates that both variants of the HMB characterise lack of cross-coupling between the position of the rotor as well as the control current in the y -axis and the magnetic force the x -axis. Visible fluctuations of the magnetic force are caused by the sensitivity of the simulation model.

Fig. 9 indicates that for both variants of the HMB change of the rotor position as well as the control current in the x -axis decreases the value of the magnetic force in the y -axis. This phenomenon is not desirable, because it destabilizes the control system. Although, it can be noticed that this negative effect occurs to a lesser extent in the variant B of the HMB.

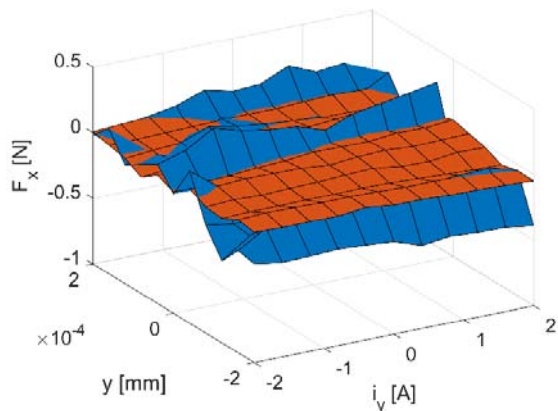


Fig. 8. The magnetic force F_x in the function of the rotor position y and the control current i_y : variant A – blue colour, variant B – red colour.

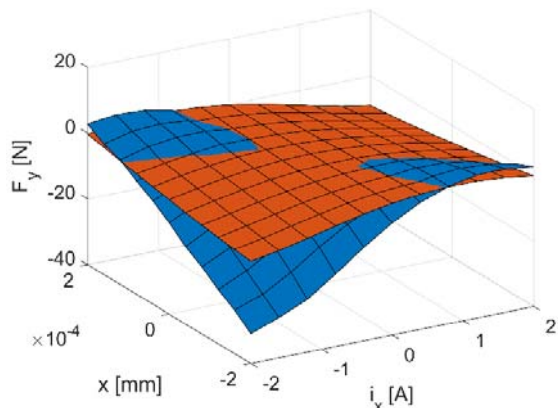


Fig. 9. The magnetic force F_y in the function of the rotor position x and the control current i_x : variant A – blue colour, variant B – red colour.

Table 2. Parameters of the variant A of the HMB

Parameter	Value
Position stiffness, k_{sx}	140.99 N/mm
Position stiffness, k_{sy}	141.21 N/mm
Current stiffness, k_{ix}	23.22 N/A
Current stiffness, k_{iy}	23.16 N/A
Initial force, F_{x0}	15.24 N
Initial force, F_{y0}	13.56 N
Maximal force, F_{xmax}	44.95 N
Maximal force, F_{ymax}	56.38 N
Force nonlinearity factor, h_{xnon}	4.05 N
Force nonlinearity factor, h_{ynon}	7.69 N
Force cross-coupling factor, h_{xc}	0.08 N
Force cross-coupling factor, h_{yc}	7.50 N
Dynamic inductance, L_d	4.95 mH
Velocity-induced voltage, e_v	18.29 Vs/m

Table 3. Parameters of the variant B of the HMB

Parameter	Value
Position stiffness, k_{sx}	105.93 N/mm
Position stiffness, k_{sy}	106.03 N/mm
Current stiffness, k_{ix}	21.97 N/A
Current stiffness, k_{iy}	22.00 N/A
Initial force, F_{x0}	21.84 N
Initial force, F_{y0}	22.53 N
Maximal force, F_{xmax}	41.84 N
Maximal force, F_{ymax}	46.09 N
Force nonlinearity factor, h_{xnon}	2.14 N
Force nonlinearity factor, h_{ynon}	2.42 N
Force cross-coupling factor, h_{xc}	0.03 N
Force cross-coupling factor, h_{yc}	2.95 N
Dynamic inductance, L_d	5.27 mH
Velocity-induced voltage, e_v	15.56 Vs/m

Parameters for both variants of the HMBs are listed in Tab. 2 and 3. Variant A of the HMB characterizes higher values of the position and current stiffness as well as higher values of initial and maximal force in relation to the variant B. Although, variant B of the HMB is marked by the lower value of force nonlinearity factors and cross-coupling factors. This feature favours the variant B of the HMB in the industry application because it simplifies the control algorithm.

Conclusions

The paper presents a comparative research of two constructions of the magnetic bearing with permanent magnets. Based on presented simulation results, variant B of the HMB is marked by lower force nonlinearity factors and cross-coupling factors in comparison to the variant A. This good feature favours the variant B of the HMB to usage in the industry application. A smaller value of the position and current stiffness of variant B of the HMB in comparison to variant A of the HMB can be compensated by increasing the length of the stator.

Author: dr inż. Dawid Wajnert, Opole University of Technology, Department of Electrical Engineering and Mechatronics, ul. Prószkowska 76, 45-758 Opole, E-mail: d.wajnert@po.edu.pl, ORCID: 0000-0001-9025-4327.

REFERENCES

- [1] Canders W-R, May H, Palka R, Topology and performance of superconducting magnetic bearings, *COMPEL – The International Journal for Computation and Mathematics in Electrical and Electronic Engineering*, 17 (1998), No. 5/6, 628-634.
- [2] Kozanecka D., Kozanecki Z., Łagodziński J., Active magnetic damper in a power transmission system, *Communications in Nonlinear Science and Numerical Simulation*, 16 (2011), No. 5, 2273-2278.
- [3] Schweitzer G., Maslen H., Magnetic bearings, theory, design, and application to rotating machinery, Springer, (2009).
- [4] Mystkowski A., Energy saving robust control of active magnetic bearings in flywheel, *Acta Mechanica et Automatica*, 6 (2012), No. 3, 72-76.
- [5] Piłat A., Active magnetic suspension and bearing, in G. Petrone and G. Cammarata, *Recent advances in modelling and simulation*, I-Tech Education and Publishing, (2008), 453-470.
- [6] Sikora B., Piłat A., Numerical model of the axial magnetic bearing with six cylindrical poles, *Archives of Electrical Engineering*, 68 (2019), No. 1, 195-208.
- [7] Graca P., Calculation and Verification of Magnetic Field Parameters in Axial Active Magnetic Bearing, *Solid State Phenomena*, 214 (2014), 143-150.
- [8] Olejnik A., Falkowski K. Passive Magnetic Bearings at the Rotary Application, Proceedings of the 9th International Conference on Rotor Dynamics, *Mechanisms and Machine Science*, 21 (2015), Springer, Cham, 1477-1487.
- [9] Falkowski K., Henzel M., High Efficiency Radial Passive Magnetic Bearing, *Solid State Phenomena*, 164 (2010), 360-365.
- [10] Mystkowski A., Investigation of Passive Magnetic Bearing with Halbach-Array, *Acta Mechanica et Automatica*, 4 (2000), No. 4, 72-76.
- [11] Okada Y. Sagawa K., Suzuki E., Kondo R., Development and Application of Parallel PM Type Hybrid Magnetic Bearings, *Journal of System Design and Dynamics*, 3 (2009), No. 9, 531-539.
- [12] Burcan J., Stawińska A., Self-controllable passive axial magnetic bearing, *Tribologia*, (2003), No. 4, 81-97.
- [13] Gosiewski Z. *Wielofunkcyjne tożyska magnetyczne*, Biblioteka Naukowa Instytutu Lotnictwa, Warszawa, (2003).
- [14] Ming Z., Yuhang L., Jixiu S., Fengxiang W., Force Analysis for Hybrid Radial Magnetic Bearing Biased by Permanent Magnet, *Proceedings of 2005 International Conference on Electrical Machines and Systems*, 27-29 September 2005, Nanjing, China, 1843-1837.

- [15] Jin Ch., Lv D., Yan X., Xiong F., Xu L., A novel eight-pole heteropolar radial-axial hybrid magnetic bearing, *International Journal of Applied Electromagnetics and Mechanics*, Vol. 60, (2019), 423-444.
- [16] Wu L., Wang D., Su Z., Wang K., Zhang X., Analytical Model of Radial PM biased Magnetic Bearing with Assist Poles, *IEEE Transactions on Applied Superconductivity*, Vol. 26, (2016), No. 7, 0610105.
- [17] Xu S., Sun J. Decoupling Structure for Heteropolar Permanent Magnet Biased Radial Magnetic Bearing With Subsidiary Air-Gap, *IEEE Transactions on Magnetics*, Vol. 50, (2014), No. 8, 8300208.
- [18] Ji L., Xu L., Jin Ch., Research on a Low Power Consumption Six-Pole Heteropolar Hybrid Magnetic Bearing, *IEEE Transactions on Magnetics*, 49 (2013), No. 8, 4918-4926.
- [19] Reisinger M., Amrhein W., Silber S., Redemann Ch., Jenckel P., Development of a low cost permanent magnet biased bearing, *Proceedings of the 9th International Symposium on Magnetic Bearings*, 3-6 August 2004, Lexington, USA.
- [20] Wajnert D., Analysis of the cross-coupling effect and magnetic force nonlinearity in the 6-pole radial hybrid magnetic bearing, *International Journal of Applied Electromagnetics and Mechanics*, Vol. 61, (2019), 43-57.
- [21] Ansoft Maxwell 3D, User Guide, Pittsburg, 2006.
- [22] Piat A., PD control strategy for 3 coils AMB, *Proceedings of the 10th International Symposium on Magnetic Bearing*, August 21-23, 2006, Martigny, Switzerland, 34-39.
- [23] Wajnert D., Tomczuk B., Koterak D., Calculation of the Magnetic Bearing Parameters, *Proceedings of 2017 International Symposium on Electrical Machines (SME 2017)*, 18-21 June 2017, Naleczow, Poland, 1-5.
- [24] Gosiewski Z., Mystkowski A., Robust control of active magnetic suspension: analytical and experimental results, *Mechanical Systems and Signal Processing*, 22 (2008), 1297-1303.
- [25] Tomczuk B., Koterak D., Waindok A., The influence of the leg cutting on the core losses in the amorphous modular transformers, *Compel - the International Journal for Computation and Mathematics in Electrical and Electronic Engineering*, 34 (2015), No. 3, 840-850.
- [26] Wajnert D., Tomczuk B., Simulation for the Determination of the Hybrid Magnetic Bearing's Electromagnetic Parameters, *Przeegląd Elektrotechniczny*, 93 (2017), Nr 2, 157-160.